Hydrated Human Corneal Stroma Revealed by Quantitative Dynamic Atomic Force Microscopy at Nanoscale

Dan Xia,[†] Shuai Zhang,[†] Jesper Østergaard Hjortdal,[‡] Qiang Li,[†] Karen Thomsen,[†] Jacques Chevallier,[§] Flemming Besenbacher,[†,§,*] and Mingdong Dong[†,*]

[†]Interdisciplinary Nanoscience Center (iNANO), Centre for DNA Nanotechnology (CDNA), Aarhus University, 8000 Aarhus, Denmark, [‡]Department of Ophthalmology, Aarhus University Hospital, 8000 Aarhus, Denmark, and [§]Department of Physics and Astronomy, Aarhus University, 8000 Aarhus, Denmark

ABSTRACT The structures and mechanical properties of human tissues are significantly influenced by water. The functionality of the human cornea can be linked to the hydrated collagen fibers. By applying quantitative dynamic atomic force microscopy to investigate morphological and mechanical property variations of corneal stroma under different hydration levels, we found that the collagen fibers in the stromal tissue show the specific periodicities and the stiffness of giga-Pa magnitude at 40% humidity. However, under increasing hydration, the collagen fibers clearly show nanoparticle structures along the fibers with the stiffness in mega-Pa magnitude. By increasing the hydration time, the stroma regains the fiber structure but with larger diameter. The age-dependency in stiffness was further investigated. The interplay of structures and nanomechanical mapping may be applied for the future diagnosis and assessment or even pathologic analysis.

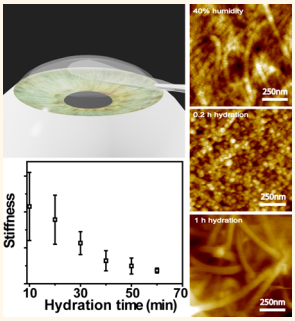

KEYWORDS: corneal stroma · hydration · mechanical property · quantitative dynamic atomic force microscopy

Water is one of the important components constituting human tissue, which accounts for ~60% of body weight for adults.[1] It is helpful in digestion and balancing body temperature. It is of paramount importance for nutrient transportation to organs and tissues, and for their proper functional structure maintenance. The cornea is one of the important connective tissues containing ~78% water, which is the convex highly transparent human tissue in the front part of the eye, covering the iris, pupil and anterior chamber.[2,3] Proper corneal function and the biophysical properties of cornea tissue depend on a precise maintenance of the hydration.

The human cornea is composed of several distinct layers including the epithelium, Bowman's layer, the stroma, Descemet's membrane and the endothelium.[4] The cornea plays important role in regulating the refractive optics of the eye and has important protective functions for the inner structures of the eye. Recent studies have focused on the biophysical characterization of these structures due to their roles in normal tissue functions and diseases.[4−10] The main part of cornea is the stroma, accounting for 90% of the corneal thickness. The corneal stroma is a very dense matrix composed of several hundred sheets of highly organized collagen lamellae lying between Bowman's layer and Descemet's membrane (Figure 1c). In the stroma extracellular matrix, collagen fibrils are arranged in a lattice-like structure and proteoglycan molecules fill the space around them.[11] Stroma has an innate tendency to imbibe fluid and a swelling capacity that exceeds any other connective tissues in the body, which is caused by a net fixed charge density created by glycosaminoglycans (a subject covalently attached to the core protein of the proteoglycan). Previous research has shown that disruption of the interfibrillar separation of stromal collagen affects stromal hydration, corneal clarity and visual acuity.[12] A normal corneal hydration is in healthy subjects provided by a normal functioning and intact layer of epithelial and endothelial cells.[13] The normal clarity of the corneal stroma is traditionally explained by destructive interference of scattered light from the interaction between collagen fibrils and interfibrillary substance (proteoglycan).[14,15] A change in hydration results in varying interfibrillary distances,

* Address correspondence to fbe@inano.au.dk, dong@inano.au.dk.

Received for review March 21, 2014 and accepted May 15, 2014.

Published online May 15, 2014
10.1021/nn5015837

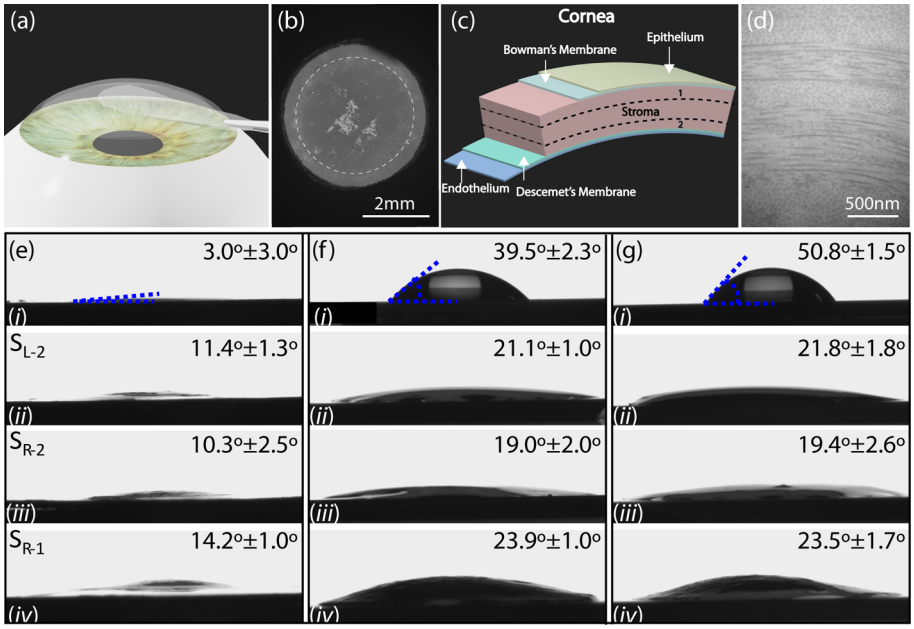

Figure 1. (a) Schematic image of excising a corneal lenticule from a corneal stroma. (b) Low magnification SEM image of the L (left eye) corneal stroma; the white dashed circle indicates the periphery of the stroma. (c) Schematic image of five parts of human cornea (the two surfaces 1 and 2 indicate the outer and inner surface of the lenticule). (d) TEM image of the cross-section of the stroma; the dashed lines indicate the boundaries between two lamella collagen layers, which have different lamella orientations. (e−g) The behavior of different corneal stromas on three different substrates, (e) mica, (f) Si and (g) SiO_2, respectively. (*i*) Contact angles of water on three different substrates and (*ii*−*iv*) the fitting angles of one pair of corneal stromas on three different substrates. S_{L-2} indicates the left corneal stroma sample with the inner surface faces up on the substrates, while S_{R-2} indicates the right corneal stroma sample with the inner surface faces up, and S_{R-1} indicates the right corneal stroma sample with the outer surface faces up.

compromised destructive interference, and therefore decreased stromal transparency, which in turn will alter corneal optics and influence the optical performance of the eye.[16] If the stromal hydration has a major departure from normal level, the visual acuity will be affected because of light scattering differences. The cornea swell is due to the attraction of water into interfibrillary substance whereby the arrangements of collagen fibrils are affected. Besides, certain diseases can also result from corneal hydration, for example, Fuchs endothelial dystrophy, pseudophakic bullous keratopathy.[17,18]

Corneal ultrastructure has been investigated extensively.[10,19−25] Numerous methods have been used to characterize the morphology, including electron microscopy,[4,5,10,26] atomic force microscopy (AFM).[4,5,27−31] The reported periodicity of the corneal collagen fiber ranged from 22 to 39 nm,[32] from 20 to 60 nm,[33] 65.7 ± 0.8 nm,[24] and 68.50 ± 10.3 nm.[27,29] Also the mechanical property of bulk cornea, including all layers, is in a wide range of stiffness values from 0.2 to 20.0 MPa.[4,30,34−38] However, the specific properties of each discrete corneal layer are not accessible by macro tensile testing or bulge testing, because of the difficulty in isolating each layer properly.

Further studies of the correlation between morphology and mechanical properties of the corneal stroma are needed to give insight into the fundamental properties on which corneal clarity depends. Recently, AFM has been shown to be an ideal technique to provide the structural information on soft biological samples at nanoscale.[39−42] In addition, AFM nanoindentation allows determining the local, mechanical properties of discrete corneal layers by measuring the modulus on the surface of the tissue and capture morphology as well.[4,30] However, the resolution of the force-volume map is poor, and the measurements are very time-consuming. To overcome this limit, an advanced quantitative dynamic AFM has been developed, which is able to record the morphology and quantitatively measure mechanical properties of inorganic and biological samples simultaneously with real-nanolateral resolution and microsecond-force identification.[41,43] So far, AFM based methods to compare the morphology and mechanical property variations of the corneal stroma under different hydration levels have not been reported.

Here, we apply quantitative dynamic AFM to investigate the structural and mechanical properties of the corneal stroma under different hydration conditions. By comparing the results, we have learned that the nanostructure and the mechanical property of the stroma are significantly influenced by the hydration levels. At 40% humidity, collagen in the corneal stroma shows a fine fiber structure. The periodicities of 24.2 ± 1.4 nm and ~67 nm coexist in the stroma tissue. The stiffness of the collagen at 40% humidity is ~7 GPa. After increasing the hydration level, the morphology of

the collagen shows particle protrusion. The Young's modulus of the collagen decreases to MPa magnitude, which are three magnitudes lower than observed at 40% humidity. With further increasing hydration level, the collagens regain the normal fiber structure but with larger fiber diameters, and the periodicity disappears. In addition, the age-dependency on corneal stiffness was preliminarily evaluated. The quantitative stiffness measurement provides a convincing rationale for evaluating the water contained to keep the cornea function. The findings encourage further research into the subjects with the ultimate perspectives of using this quantitative dynamic AFM approach to diagnose and characterize corneal diseases by examining the stiffness differences of the cornea and tissue in general.

RESULTS AND DISCUSSION

Corneal lenticules were excised by a femtosecond laser in ReLEx SMILE surgery[44] for myopia (Figure 1a and Supporting Information Figure S1). The transparent part clamped by the forcep is the removed lenticule from the bulk stroma at a depth of approximately 120 μm from the corneal surface. The low magnification scanning electron microscope (SEM) image (Figure 1b) shows the removed lenticule on a mica surface. The white dashed circle indicates the periphery of the lenticule. The thickness of the removed lenticule depends on the degree of myopia being treated, while the diameter ranges from 6.0 to 6.5 mm. The removed lenticule from the corneal stroma is also demonstrated in the schematic image of the layer structure of the stroma as the part between the two dark dash lines (1 and 2) shown in Figure 1c, where the five parts of cornea are illustrated. The stroma accounts for 90% thickness of the whole cornea (the pink part of cornea in Figure 1c), where *stroma_1*/*stroma_2* indicate the outer/inner surface of the lenticule, respectively. The detailed structure of the surface and cross-section of the stromal samples are revealed by high resolution SEM (Supporting Information Figure S2) and transmission electron microscopy (TEM) (Figure 1d and Supporting Information Figure S3), where the highly ordered interweave lamellar structure is clearly seen.

The hydrophilicity/hydrophobicity of the stroma can be evaluated by depositing the stroma onto different substrates (mica, Si_silicon, SiO_2_silicon oxide) with different hydrophobicity. The contact angles of water drops on three bare fresh substrates (3.0°, 39.5°, 50.8°) represent the degree of hydrophobicity (Figure 1e−g, *i*). It illustrates that mica is the most hydrophilic, while Si and SiO_2 are less hydrophilic. The stromas were transferred onto these three different substrates to investigate the shape changes (Figure 1e−g, *ii*−*iv*). Here the shape of the contour of corneal stromas deposited on these substrates is fitted and the relative fitting angles are measured (labeled on the images). The results show that the stroma deposited on mica surface is more stretched comparing to that on silicon or silicon oxide substrates. That is because the stroma contains high water level and the mica surface is very hydrophilic, thus the stroma will reshape immediately like water after it is deposited on the mica substrate, and it was stretched to be flat. Because of the more hydrophobic properties of the Si/SiO_2 substrates, the fitting angles of the stroma onto them are larger (on mica substrate: ~10°; on Si and SiO_2: ~20°). The fitting angles of one pair of stromas on three substrates are shown in Figure 1e−g, *ii, iii*. Both $S_{L\text{-}2}$ and $S_{R\text{-}2}$ perform very similarly on the same kind of substrate (on mica, L, 11.4° ± 1.3°, R, 10.3° ± 2.5°; on silicon, L, 21.1° ± 1.0°, R, 19.0° ± 2.0°; on silicon oxide, L, 21.8° ± 1.8°, R, 19.4° ± 2.6°). This demonstrates no major topographical differences between L and R corneal stromas on the same substrate. However, for $S_{R\text{-}2}$ and $S_{R\text{-}1}$ samples (Figure 1e−g, *iii, iv*), the fitting angles of $S_{R\text{-}1}$ are larger than that of $S_{R\text{-}2}$ because of the inherent curvature of the cornea stroma. These different behaviors of the stroma onto different substrates must be linked with the high water containing and the unique interweave lamella packing structures (Figure 1d and Supporting Information Figures S2, S3). It is also believed that this may be tightly related to the mechanical property of the cornea stroma.

These observations suggest that the water in the stroma is important to keep the inherent shape. However, what will happen when the stromal water content is reduced? How about the structure and the physical property? In order to answer these questions, the corneal stroma properties are investigated at extreme condition-ambient condition (40% humidity). The AFM images of $S_{L\text{-}1}$, $S_{L\text{-}2}$ and $S_{R\text{-}2}$ samples are shown in Supporting Information Figure S4. It is shown that the morphologies of these three samples are very similar and there are no obvious morphological variations between the corneas from both eyes and the two sides of individual ones. The high resolution AFM images in Supporting Information Figure S4c,f,i, further show that the corneal stroma is composed of fine collagen fibers which are the main component of the cornea.[45]

To investigate the nanostructure of the collagen fiber in detail, high resolution AFM imaging (Figure 2a and Supporting Information Figure S5) was further carried out. The periodicity of the fibers can be clearly seen in these images. The line profiles of five collagen fibers in different colors in Figure 2a are shown in Figure 2b. By dividing the fiber length over the bump length, the periodicity of individual fiber is calculated, ranging from 24.9 to 28.0 nm. Also, the periodicities of fibers in $S_{L\text{-}1}$ and $S_{R\text{-}2}$ corneal stromas were analyzed, respectively (Supporting Information Figure S5). The inset in Figure 2a is a Fast Fourier transformation (FFT) of the topography to analyze repeated patterns. Fourier images reflect repeated patterns as narrow peaks, the coordinates of which describe their periodicity and

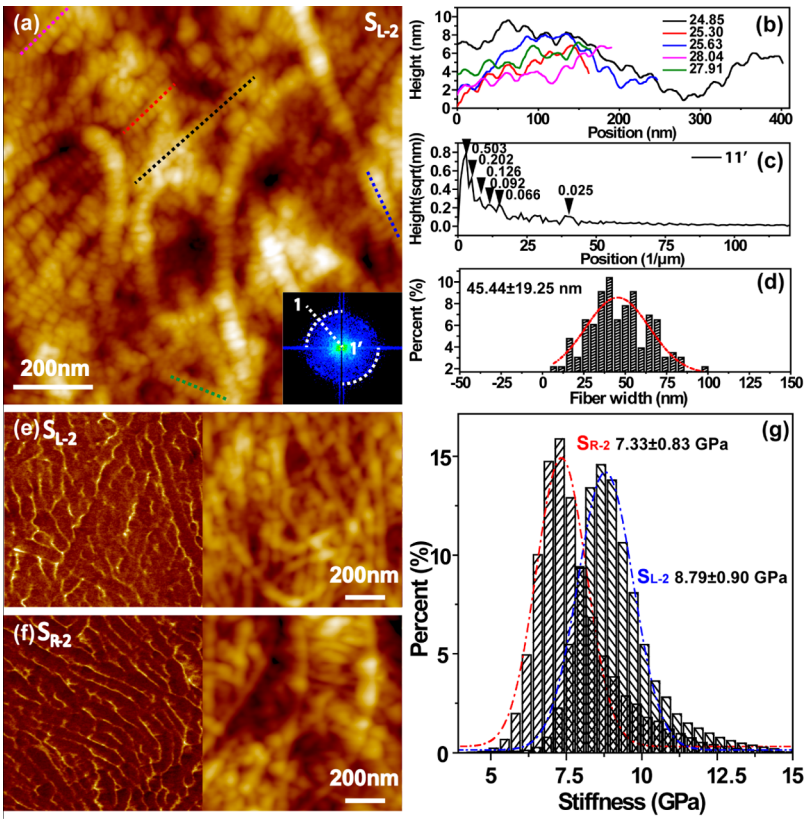

Figure 2. Periodicity and Young's modulus of the corneal stroma. (a) AFM morphology image of S_{L-2}. The inset is the FFT image of (a); the arc line indicates the outmost circle of the FFT pattern. (b) The profiles of five color lines in (a). (c) The line profile of 11′ in the inset of (a). (d) The fiber width distribution of the collagen fiber in (a). (e,f) The stiffness maps of S_{L-2} and S_{R-2}; the right parts of both images are covered by the topography images. (g) The distribution of Young's moduli of both samples.

direction. The repeat distances can be measured very accurately by determining the Fourier peak coordinates at subpixel level. The white dashed curves in the inset indicate the outmost circle of the FFT pattern. The line profile of 11′ in Figure 2c indicates the periodicity of collagen fibers. The coordinates along the *x*-axis shown in Figure 2c should be multiple of the periodicity. And the outmost circle of the Fourier transformation pattern (inset of Figure 2a) corresponds to the last peak in Figure 2c, which is supposed to be the minimum repetition period. It turns out the periodicity is ~25.0 nm, which is consistent with the value (24.2 ± 1.4 nm) obtained from the line scan analysis. Moreover, the width of the collagen fiber was analyzed as well. The distribution of the fiber width and the Gaussian fitting (Figure 2d) show the width of the collagen fiber is around 45.4 nm. The fiber widths of both S_{L-2} and S_{R-2} (Supporting Information Figure S6) are almost the same. These results are consistent with previous cornea studies by AFM that the periodicities of corneal stroma is ranged from 22 to 39 nm,[32] from 20 to 60 nm.[33] However, it is different from the well-known D-banded structure (the periodicity of around 68 nm[27,29,46,47]), which can be assembled from tropocollagen through controlling the collagen concentration, incubation time, temperature and pH.[48−50]

Interestingly, the D-banded periodicity was clearly observed at the brim of the stroma samples where both the isolated and bulk collagen can be identified (Figure 3a). Figure 3b and Supporting Information Figure S7a are zoomed in from the dashed squares in Figure 3a, where the isolated collagen or the bulk collagen is dominant, respectively. The morphology images (Figure 3b, Supporting Information Figure S7a) and the corresponding line profiles of 11′ (Figure 3e) and 33′ (Supporting Information Figure S7b) show two distinct periodicities (61.6 and 23.2 nm), respectively. In addition, the line profiles of aa′ and bb′ (Figure 4g, Supporting Information Figure S7c) derived from the FFT images (the insets of Figure 4b, Supporting Information Figure S7a) of the morphology images are shown coexisting these two periodicities both in isolated and bulk collagen of the tissue. More interestingly, combining the morphology (Figure 3b) and the *in situ* phase image (Figure 3c) of the isolated collagen, it is found that the higher periodicity (~62 nm indicated in the line profile of Figure 3e) is composed of three small periodicities (~21 nm indicated in the line profile of Figure 3f). The periodicity of the D-band structure of the isolated collagen is also found to be ~67 nm (Supporting Information Figure S7d−j), which is composed of three ~22 nm periodicities.

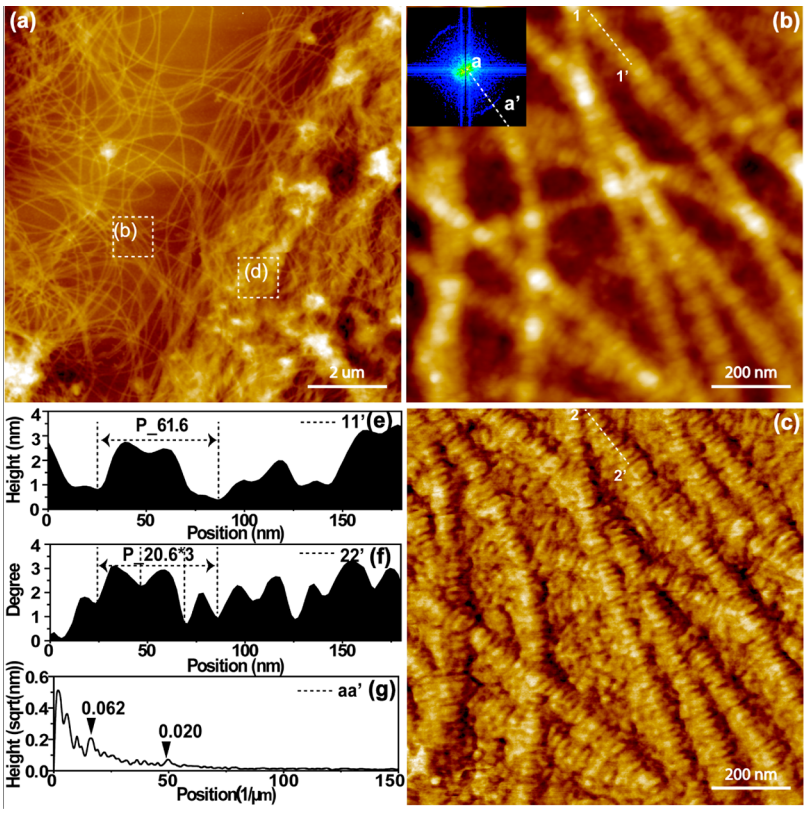

Figure 3. (a) The morphology of the stroma sample at the brim. (b,d) The zoomed in images from the dash squares in (a); the insets are the corresponding FFT images. (c) The *in situ* phase image of (b). (e,f) The line profiles of 11′, and 22′ in (b−c), respectively (*P* indicates the periodicity). (g) The line profiles of aa′ in the inset of (b).

It is apparently observed the clear fingerprint of D-band (~67 nm periodicity) when the collagen is isolated compared with the high roughness of bulk stroma.

Beside of nanostructure study, quantitative nanomechanical measurements provided further physical properties of stroma. Figure 2e,f shows the stiffness maps of $S_{L\text{-}2}$ and $S_{R\text{-}2}$ corneal stromas, respectively. Both the right halves of the maps are covered by the topography images. In stiffness maps, the color contrast represents the stiffness instead of the height: the brighter means the stiffer and vice versa. The stiffness maps show that the mechanical properties of both corneal stromas are very homogeneous. Here, one can see that the $S_{L\text{-}2}$ is slightly stiffer than the $S_{R\text{-}2}$, but histograms are overlapped partially, which means there are no larger stiffness differences between these stromal samples. The stiffness of $S_{R\text{-}1}$ is shown in Supporting Information Figure S8. Compared with $S_{R\text{-}2}$, the stiffness values of both samples are almost the same. It is concluded that the nanostructure and mechanical property of both L and R corneal stromas and of both inner and outer surfaces of the same stroma are independent of physical positions under ambient condition.

From the mechanics viewpoint, the corneal stroma is a polyelectrolyte gel, which will swell when it is immersed in a solution. The swelling tendency for the stroma to imbibe water is higher compared to other connective tissues due to the imbalance between the ionic concentration inside and outside of the tissue. The morphologies of the stroma in water and physiological buffer with different hydration time were studied. Figure 4a,b shows the topography images of a human corneal stromal lenticule immersed in water for 0.2 h. It is clear that the topography of the hydrated stroma with the particles along the fibers is different from that under the 40% humidity condition. The sizes of particles along the fibers are heterogeneous, which means the initial swelling process is nonuniform. This may be because the proteoglycan composition (chondroitin sulfate, keratan sulfate and dermatan sulfate) has the different capacity of water swelling.[51] However, the periodicity of the collagen fiber is hard to distinguish in AFM images. Figure 4c shows the line profile of 11′ based on the inset in Figure 4b (the FFT of the topography of Figure 4b), in which the periodicity of the repeating pattern on hydrated stroma can be indicated. The results show 22.0 and 65.0 nm repeating units, consistent with the collagen fiber periodicity in 40% humidity condition. Moreover, the particle size is also analyzed. The particle size distribution derived from the fitting image (Supporting Information Figure S6) shows the value is around 21.0 nm (Figure 4d). The morphology of the stromal tissue in physiological buffer after being

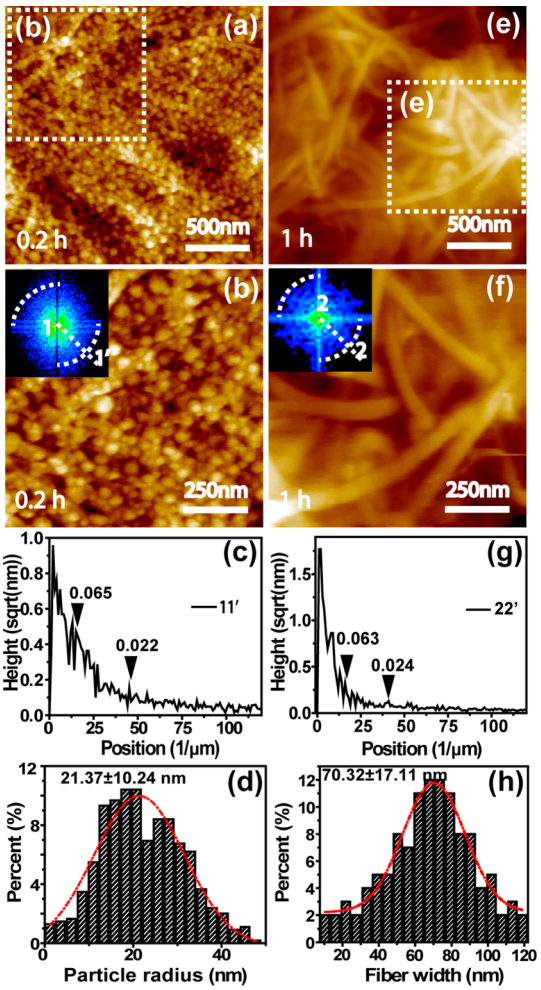

Figure 4. AFM morphology images of corneal stroma in liquid. (a) The AFM images of corneal stroma immersed in water for 0.2 h. (b) The zoomed in image from the dashed square in (a). (e) AFM images of corneal stroma after 1 h immersed in physiological buffer. (f) The zoomed in image from the dashed square in (e). The insets in (b) and (f) are the FFT images of their topography images; the arc lines indicate the outmost circle of the FFT spots. (c,g) The line profiles of 11′ and 22′ in the insets of (b) and (f). (d) The particle radius distribution of corneal stroma. (h) The fiber width of the collagen fiber.

immersed for 0.2 h is very similar to that in water condition (Supporting Information Figure S9), which indicates the ion concentration has little effect on the swelling morphology of stroma.

In corneal stroma, a very small portion of stromal fluid is directly related to the collagen fibrils hydration, and the rest of the fluid interpenetrates between the collagen fibrils to keep the fibrils apart. Therefore, the increasing amount of fluid associated with increasing hydration pushes the fibrils further apart and weakens the neighboring fibrils interaction resulting in the stroma swell.[2] Interestingly, the morphologies of the stroma immersed in physiological buffer for 1 h regain fiber structure (Figure 4e,f). The particle protrusions on the fiber disappear. But the fibers are much larger than these in 40% humidity and in liquid condition with short hydration time (0.2 h). Similar to that under liquid condition with short hydration time, no apparent periodicity is distinguished. But the line profile of 22′ based on the inset in Figure 4f (the FFT of the topography of Figure 4f) shows that the repeating patterns are around 24.0 and 63.0 nm. In addition, the fiber width of the collagen fiber in physiological buffer is around 70 nm (Figure 4h), much wider than that in 40% humidity. The increasing of the fiber width is important to contribute the swell. Moreover, the stroma samples here are denuded of the epithelium and the endothelium (Figure 1c). The ion transport function of endothelial cells counteracts corneal tendency to swell is disabled.[52] It may induce the further swell. The image of the stroma tissue dried out after imaging in liquid shows regular periodicity as well (Supporting Information Figure S10), which indicates that the wetting process is reversible.

Considering that structural changes are often related to the corresponding mechanical property changes, the comparison of corresponding mechanical properties of corneal stroma under different hydrations is studied. The topography images superimposed the stiffness maps of the same stroma under different hydrations are shown in Figure 5a–c. The force–distance curves recorded on the stroma samples under three different hydration conditions are shown in Figure 5d–f, respectively. The force spectroscopy under the controlled force enabled a quantification of the local deformation to allow investigations without the stroma bulk involved. It is shown the local deformations (indentations) of the sample in water (0.2 h hydration) and in physiological buffer (1 h hydration) are ~15 and ~50 nm, respectively. Compared with the thickness (~140 μm) of the whole stroma, these deformations are fully negligible. Hence, the overall deformation of the stroma and the substrate effect will not contribute to the measured Young's moduli. It is obvious that the corneal stroma at 40% humidity forms linear force–distance curves, while it forms nonlinear force–distance curves in liquid. This linear/nonlinear behavior is demonstrated by the slops of force–distance curves. Under 40% humidity condition, the slope is almost consistent along with the indentation, while it is varied in liquid. The indentation for full hydration sample can reach up to 50 nm with 3 nN loading force (Figure 5f). However, the maximum indentation for 40% humidity in a sample is only ~5 nm even with ~50 nN loading force applied (Figure 5d). This ~10 times larger indentation presents the possible large deformation of particles-shape and bigger collagen fibers in the stroma after the hydration and indicates containing the high amount of water.

Obviously, under fully hydrated conditions, the swollen stroma leads to a viscoelastic model.[53,54] Meanwhile, the swollen stroma exhibits some dissipative behavior, which is manifested as a loss of some

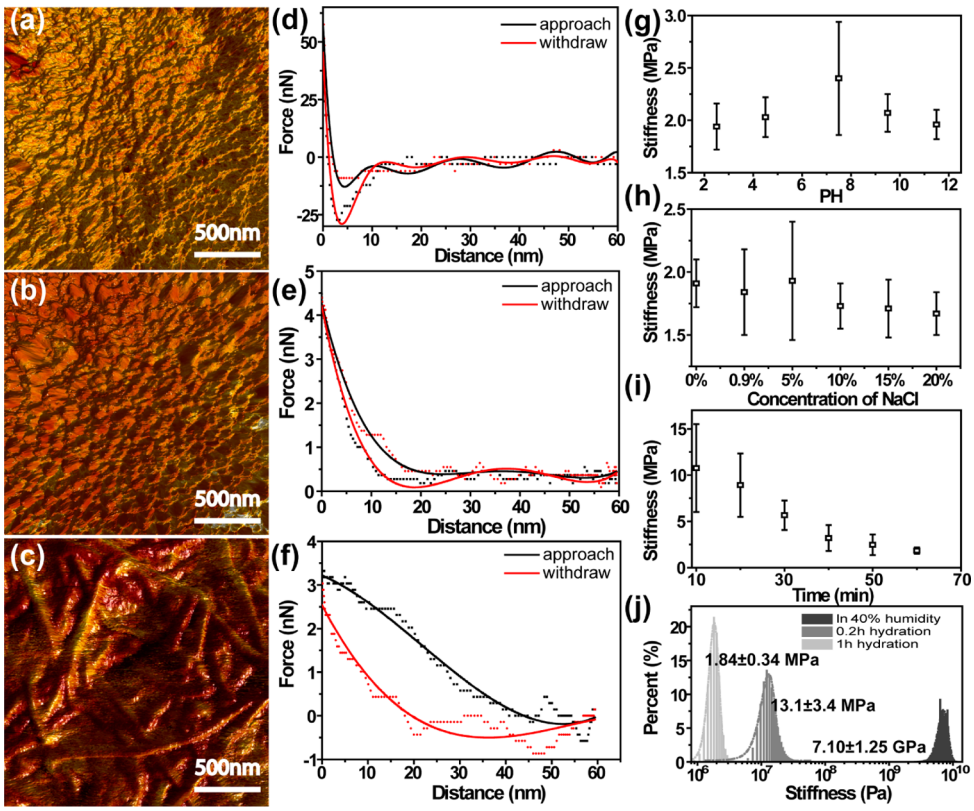

Figure 5. Stiffness map superimposed with the topography image of corneal stroma (a) under 40% humidity, (b) under 0.2 h hydration time and (c) under 1 h hydration time. (d–f) The representative force–distance curves of the corneal stroma according to different hydration levels. The stiffness *versus* the (g) pH, (h) concentration of NaCl solution and (i) hydration time. (j) The comparison of the stiffness distributions of corneal stroma under different hydration levels.

energy stored during loading. It can be seen in the indentation process as hysteresis in a cycle of force displacement (Figure 5f), which is much larger than that under 40% humidity. This energy dissipation is believed to be accomplished by internal friction and/or viscous damping mechanisms.[55,56]

Considering the different composition of water and physiological buffer, several control experiments were initiated. The Young's moduli of the stroma under different pH conditions are shown in Figure 5g. Generally speaking, the pH value has little effect on the stiffness of the stroma. The stiffness is around 2 MPa. Also, the stiffness values of the stroma in NaCl solutions with different concentration were investigated (Figure 5h). No large changes were observed. Interestingly, the stiffness of the stroma changes a lot with the variation of hydration time in physiological buffer, shown in Figure 5i. The stiffness of the stroma decreases monotonically with increasing hydration time and then becomes saturated, which means that the hydration level plays significant role to the mechanical properties of stroma. The relative stiffness distributions of corneal stroma, according to the stiffness maps (Figure 5a–c) and the force–distance curves (Figure 5d–f) under different hydration levels are given (Figure 5j). Apparently, the stiffness of stroma in 40% humidity is two/three magnitudes higher than that of the 0.2 h/1 h hydrated corneal stroma. During the hydration process, the total fixed charge density of the stroma, electrostatic repulsion between glycosaminoglycans and the osmotic pressure decrease.[11] Any decrease in the osmotic pressure possibly decreases the prestress of collagen fibrils to change the stroma stiffness. It is of huge difference just because of the various hydration levels. So maintenance the normal level of hydration in human eye is critical to keep its functionality.

The mechanical behavior of the stroma under different hydration levels suggests that the stiffness may be used for evaluating biological functionalities of tissue materials. Total body water demonstrates a diminution trend with increasing age.[57] So does the corneal hydration control.[58] The aging effect on the mechanical properties of corneal stromas from different donors (6-, 25-, 41-year-old patients, respectively) was investigated. Both topographies (Supporting Information Figure S5e,g,i) and periodicities (22.0–25.0 nm Supporting Information Figure S5f,h,j) of these three samples are similar. The stiffness maps superimposed with the morphology (Supporting Information Figure S11a–c) with the corresponding distribution (Supporting Information Figure S11d) of these three samples show that age has a significant effect on the mechanical properties of the corneal stroma under the

same hydration condition. Just as reported previously, the human tissue including human lens and the cornea stiffen with age.[59−61] The mechanical distributions of these three samples shift to the higher stiffness value with increasing age. Besides, the full width half-maximum of modulus distributions becomes broader over age, which indicates that the stiffness of the stroma becomes less and less homogeneous. The mechanical property change of corneal stroma over age may either be caused by a change of the hydration or a change in interfibrillar structure or cohesion.[58,61,62]

CONCLUSION

The structure and mechanical properties of the lenticules of corneal stroma removed by a femtosecond laser corneal surgery from healthy human subjects under different hydration level conditions have been investigated by quantitative dynamic AFM, which allows us to learn the morphology and stiffness of the corneal stroma in a quantitative and correlation way. Experimental results show that the structure and the stiffness of corneal stroma are significantly different under different hydration levels. Under 40% humidity ambient condition, collagen shows a fine fiber structure with both of 24.2 ± 1.4 nm and of ∼67 nm periodicities. The large periodicity (∼67 nm) is composed of three small periodicities (∼22 nm). Corneal stroma at 40% humidity ambient condition is very stiff with the stiffness in GPa magnitude, which is consistent with the stiffness of the collagen in air-dry condition.[43] However, under hydration condition, the morphology of the collagen shows some particles along the fiber and the apparent periodicity disappears. Most interestingly, the Young's modulus of the collagen drops down to MPa magnitude, 3 orders of magnitude softer than that in 40% humidity condition. With increasing hydration time, the collagen regains fiber structure but with larger size, and no apparent periodicity can be identified. It is necessary to realize the hydration effect on the fibers' size. This proves the stroma has an innate tendency to imbibe fluid, and its biophysical property depends on precisely maintaining its hydration level. In addition, the aging effect may be discriminated by this technique in terms of the stiffness. Both swelling effects and stiffness changes of stroma are due to an innate tendency of the stromal tissue to imbibe fluid. This unusual connective tissue is able to provide the possible controlling the water level to avoid the light scatting. Since the corneal stroma shows significant different mechanical properties under different conditions, this technique provides the possibility of diagnosing and assessing diseases associated with stiffness changes due to the collagen defects and disorder. Also, quantitative stiffness measurements may be applied to investigate other clinic human tissues and organs.

METHODS

Samples Preparation. The stroma samples (lenticules) were from ReLEx SMILE surgery,[44] which remodels the profile of the cornea by removing the stroma to correct myopia (nearsightedness), supplied by Aarhus University Hospital, Denmark. After corneal surgery, the samples were kept in the 0.9% NaCl solution and were further used in the fitting angle, SEM and AFM characterization.

"Fitting Angle" Measurement. The contact angle of the three substrates and the fitting angles of the cornea samples on three different substrates were measured with a drop shape analysis system (Krüss DSA100) in the sessile mode at room temperature. All reported contact angles were the average of five measurements.

SEM Analysis. *Low Magnification SEM.* Cornea samples on mica surface were characterized by low magnification SEM. Before this measurement, the sample was mounted on an aluminum holder with double-sided adhesive tape. SEM micrographs were taken on a Hitachi TM-1000 tabletop microscope, maximum accelerating voltage of 15 kV.

High Magnification SEM. After the critical point drying, the morphology of the cornea stroma was determined by high-resolution SEM (FEI, Nova 600 NanoSEM). The SEM was operated in low vacuum mode because of the nonconductive property of the sample.

TEM Analysis. The samples are fixed in 2% glutaraldehyd and 0.1 M cacodylate solution immediately after being removed from the patient. TEM (CM 100) was applied to reveal the micro- and nanostructures of the samples.

Quantitative Dynamic AFM Measurement. The AFM images and quantitative mechanical measurements were recorded with Peakforce Tapping mode in a commercial Nanoscope VIII MultiMode SPM system (Bruker, Santa Barbara, CA) under both ambient (temperature, 24 °C; humidity, 40%) and liquid (different concentrations of NaCl solutions, PBS buffer at the different pH values) conditions. For the air measurements, the cornea samples were deposited onto the freshly cleaved mica surface, air-dried. Ultrasharp silicon tips (rectangular, TESP-SS, Bruker) with a standard spring constant of 20−80 N/m and a normal tip radius of 2 nm were used for imaging morphology. The silicon tips (rectangular, MPP-13120−10, recommended stiffness measurement range: 1 GPa < E < 20 GPa, Bruker) with a standard spring constant of 200 N/m and a normal tip radius of 8 nm was used for mechanical measurement. For the liquid measurements, the cornea was mechanically fixed onto the mica surface and immersed by the liquid while scanning. The silicon tips (rectangular, MPP-12120−10, recommended stiffness measurement range: 5 MPa < E < 500 MPa, Bruker) with a standard spring constant of 5 N/m and a normal tip radius of 8 nm and the silicon tips (triangular, FastScan C, spring constant: 0.4−1.2 N/m, Bruker) with a normal tip radius of 5 nm were used for morphology and mechanical measurement for hydrated samples.

Data Analysis. All the images and size distribution were analyzed by using the commercial software Scanning Probe Image Processor (SPIP). All force curves were analyzed with offline software NanoScope Analysis (Bruker, Santa Barbara, CA).

Conflict of Interest: The authors declare no competing financial interest.

Acknowledgment. The authors gratefully acknowledge the financial support from the Danish National Research Foundation and the National Natural Science Foundation of China to the Sino-Danish Center of excellence on "The Self-assembly and Function of Molecular Nanostructures on Surfaces", from the Danish Research Councils for the support to the Interdisciplinary Nanoscience (iNANO) Center and from the

Carlsberg Foundation. D.X. acknowledges Ph.D. Scholarship from China Scholarship Council of the Ministry of Education of China. M.D. acknowledges a STENO grant from the Danish Research Council and the Young Investigator Program from the Villum Foundation.

Supporting Information Available: The scheme and photo image of stroma preparation by the femtosecond laser corneal surgery (Figure S1); the high resolution SEM images of the sample (Figure S2); the TEM images of the cross-section of stroma samples (Figure S3); AFM morphology images of $S_{L\text{-}1}$, $S_{L\text{-}2}$ and $S_{R\text{-}2}$ stroma samples (Figure S4); the line profiles of $S_{L\text{-}1}$ and $S_{R\text{-}2}$ and aging effect samples (Figure S5); the fiber width and particle radius analysis fitted images and the relative distribution (Figure S6); the morphology and the periodicities of the bulk and isolated collagen (Figure S7); the mechanical property of $S_{R\text{-}1}$ sample (Figure S8); the morphology of the stroma in physiological buffer (Figure S9); the morphology of the air-dried stroma after imaging in liquid (Figure S10); the aging effect on the mechanical property of stroma samples (Figure S11). This material is available free of charge *via* the Internet at http://pubs.acs.org.

REFERENCES AND NOTES

1. Jequier, E.; Constant, F. Water as an Essential Nutrient: The Physiological Basis of Hydration. *Eur. J. Clin. Nutr.* **2009**, *64*, 115–123.
2. Hodson, S. A. Corneal Stromal Swelling. *Prog. Retinal Eye Res.* **1997**, *16*, 99–116.
3. Davson, H. The Hydration of the Cornea. *Biochem. J.* **1955**, *59*, 24–28.
4. Last, J. A.; Liliensiek, S. J.; Nealey, P. F.; Murphy, C. J. Determining the Mechanical Properties of Human Corneal Basement Membranes with Atomic Force Microscopy. *J. Struct. Biol.* **2009**, *167*, 19–24.
5. Abrams, G. A.; Schaus, S. S.; Goodman, S. L.; Nealey, P. F.; Murphy, C. J. Nanoscale Topography of the Corneal Epithelial Basement Membrane and Descemet's Membrane of the Human. *Cornea* **2000**, *19*, 57–64.
6. Meek, K. M.; Boote, C. The Organization of Collagen in the Corneal Stroma. *Exp. Eye Res.* **2004**, *78*, 503–512.
7. Oliveira-Soto, L.; Efron, N. Morphology of Corneal Nerves Using Confocal Microscopy. *Cornea* **2001**, *20*, 374–384.
8. Olivier, N.; Aptel, F.; Plamann, K.; Schanne-Klein, M.-C.; Beaurepaire, E. Harmonic Microscopy of Isotropic and Anisotropic Microstructure of the Human Cornea. *Opt. Express* **2010**, *18*, 5028–5040.
9. Patel, D. V.; McGhee, C. N. J. *In Vivo* Confocal Microscopy of Human Corneal Nerves in Health, in Ocular and Systemic Disease, and Following Corneal Surgery: A Review. *Br. J. Ophthalmol.* **2009**, *93*, 853–860.
10. Sabater, A. L.; Guarnieri, A.; Espana, E. M.; Li, W.; Prósper, F.; Moreno-Montañés, J. Strategies of Human Corneal Endothelial Tissue Regeneration. *Regener. Med.* **2013**, *8*, 183–195.
11. Hatami-Marbini, H. Hydration Dependent Viscoelastic Tensile Behavior of Cornea. *Ann. Biomed. Eng.* **2014**, 1–9.
12. Patel, S.; Alió, J. L.; Pérez-Santonja, J. J. Refractive Index Change in Bovine and Human Corneal Stroma before and after Lasik: A Study of Untreated and Re-Treated Corneas Implicating Stromal Hydration. *Invest. Ophthalmol. Visual Sci.* **2004**, *45*, 3523–3530.
13. Maurice, D. M. The Structure and Transparency of the Cornea. *J. Physiol.* **1957**, *136*, 263–286.
14. Fatt, I.; Harris, M. Refractive Index of the Cornea as a Function of Its Thickness. *Am. J. Optom. Arch. Am. Acad. Optom.* **1973**, *50*, 383.
15. Laing, R. A.; Sandstrom, M. M.; Berrospi, A. R.; Leibowitz, H. M. Changes in the Corneal Endothelium as a Function of Age. *Exp. Eye Res.* **1976**, *22*, 587–594.
16. Kostyuk, O.; Nalovina, O.; Mubard, T. M.; Regini, J. W.; Meek, K. M.; Quantock, A. J.; Elliott, G. F.; Hodson, S. A. Transparency of the Bovine Corneal Stroma at Physiological Hydration and Its Dependence on Concentration of the Ambient Anion. *J. Physiol.* **2002**, *543*, 633–642.
17. Gaynes, B.; Oshinskie, L. Pseudophakic Bullous Keratopathy. *J. Am. Optom. Assoc.* **1985**, *56*, 794–796.
18. Borboli, S.; Colby, K. Mechanisms of Disease: Fuchs' Endothelial Dystrophy. *Ophthalmol. Clin. North Am.* **2002**, *15*, 17–25.
19. Mandell, R. B.; Fatt, I. Thinning of the Human Cornea on Awakening. *Nature* **1965**, *208*, 292–293.
20. Vaughan, J. M.; Randall, J. T. Brillouin Scattering, Density and Elastic Properties of the Lens and Cornea of the Eye. *Nature* **1980**, *284*, 489–491.
21. Munier, F. L.; Korvatska, E.; Djemai, A.; Paslier, D. L.; Zografos, L.; Pescia, G.; Schorderet, D. F. Kerato-Epithelin Mutations in Four 5q31-Linked Corneal Dystrophies. *Nat. Genet.* **1997**, *15*, 247–251.
22. Irvine, A. D.; Corden, L. D.; Swensson, O.; Swensson, B.; Moore, J. E.; Frazer, D. G.; Smith, F. J. D.; Knowlton, R. G.; Christophers, E.; Rochels, R.; *et al.* Mutations in Cornea-Specific Keratin K3 or K12 Genes Cause Meesmann's Corneal Dystrophy. *Nat. Genet.* **1997**, *16*, 184–187.
23. Le, Q.; Deng, S. X.; Xu, J. *In Vivo* Confocal Microscopy of Congenital Aniridia-Associated Keratopathy. *Eye* **2013**, *27*, 763–766.
24. Ahn, W.; Hong, H.; Zhang, M.; Chung, E.; Son, Y. Induction of Mesenchymal to Epithelial Transition of Circulating Mesenchymal Stem Cells by Conditioned Medium of Injured Cornea. *Tissue Eng. Regener. Med.* **2013**, *10*, 86–92.
25. Hjortdal, J. Ø.; Jensen, P. K. *In Vitro* Measurement of Corneal Strain, Thickness, and Curvature Using Digital Image Processing. *Acta Ophthalmol. Scand.* **1995**, *73*, 5–11.
26. Komai, Y.; Ushiki, T. The Three-Dimensional Organization of Collagen Fibrils in the Human Cornea and Sclera. *Invest. Ophthalmol. Visual Sci.* **1991**, *32*, 2244–2258.
27. Yamamoto, S.; Hitomi, J.; Sawaguchi, S.; Abe, H.; Shigeno, M.; Ushiki, T. Observation of Human Corneal and Scleral Collagen Fibrils by Atomic Force Microscopy. *Jpn. J. Ophthalmol.* **2000**, *44*, 318.
28. Serrao, S.; Buratto, L.; Lombardo, G.; De Santo, M. P.; Ducoli, P.; Lombardo, M. Optimal Parameters to Improve the Interface Quality of the Flap Bed in Femtosecond Laser-Assisted Laser *In Situ* Keratomileusis. *J. Cataract Refractive Surg.* **2012**, *38*, 1453–1459.
29. Meller, D.; Peters, K.; Meller, K. Human Cornea and Sclera Studied by Atomic Force Microscopy. *Cell Tissue Res.* **1997**, *288*, 111–118.
30. Lombardo, M.; Lombardo, G.; Carbone, G.; De Santo, M. P.; Barberi, R.; Serrao, S. Biomechanics of the Anterior Human Corneal Tissue Investigated with Atomic Force Microscopy. *Invest. Ophthalmol. Visual Sci.* **2012**, *53*, 1050–1057.
31. Ziebarth, N. M.; Dias, J.; Hürmeriç, V.; Shousha, M. A.; Yau, C. B.; Moy, V. T.; Culbertson, W. W.; Yoo, S. H. Quality of Corneal Lamellar Cuts Quantified Using Atomic Force Microscopy. *J. Cataract Refractive Surg.* **2013**, *39*, 110–117.
32. Matteini, P.; Sbrana, F.; Tiribilli, B.; Pini, R. Atomic Force Microscopy and Transmission Electron Microscopy Analyses of Low-Temperature Laser Welding of the Cornea. *Laser Med. Sci.* **2009**, *24*, 667–671.
33. Fullwood, N. J.; Hammiche, A.; Pollock, H. M.; Hourston, D. J.; Song, M. Atomic Force Microscopy of the Cornea and Sclera. *Curr. Eye Res.* **1995**, *14*, 529–535.
34. Hjortdal, J. Ø. Extensibility of the Normo-Hydrated Human Cornea. *Acta Ophthalmol. Scand.* **1995**, *73*, 12–17.
35. Hjortdal, J. Ø. Regional Elastic Performance of the Human Cornea. *J. Biomech.* **1996**, *29*, 931–942.
36. Jayasuriya, A. C.; Ghosh, S.; Scheinbeim, J. I.; Lubkin, V.; Bennett, G.; Kramer, P. A Study of Piezoelectric and Mechanical Anisotropies of the Human Cornea. *Biosens. Bioelectron.* **2003**, *18*, 381–387.
37. Liu, J.; Roberts, C. J. Influence of Corneal Biomechanical Properties on Intraocular Pressure Measurement: Quantitative Analysis. *J. Cataract Refractive Surg.* **2005**, *31*, 146–155.
38. Nash, I. S.; Greene, P. R.; Foster, C. S. Comparison of Mechanical Properties of Keratoconus and Normal Corneas. *Exp. Eye Res.* **1982**, *35*, 413–424.
39. Dong, M.; Husale, S.; Sahin, O. Determination of Protein Structural Flexibility by Microsecond Force Spectroscopy. *Nat. Nanotechnol.* **2009**, *4*, 514–517.

40. Dong, M.; Sahin, O. A Nanomechanical Interface to Rapid Single-Molecule Interactions. *Nat. Commun.* **2011**, *2*, 247.
41. Lazar, P.; Zhang, S.; Šafářová, K.; Li, Q.; Froning, J. P.; Granatier, J.; Hobza, P.; Zbořil, R.; Besenbacher, F.; Dong, M.; *et al.* Quantification of the Interaction Forces between Metals and Graphene by Quantum Chemical Calculations and Dynamic Force Measurements under Ambient Conditions. *ACS Nano* **2013**, *7*, 1646–1651.
42. Song, J.; Arbona, J.-M.; Zhang, Z.; Liu, L.; Xie, E.; Elezgaray, J.; Aime, J.-P.; Gothelf, K. V.; Besenbacher, F.; Dong, M. Direct Visualization of Transient Thermal Response of a DNA Origami. *J. Am. Chem. Soc.* **2012**, *134*, 9844–9847.
43. Liu, Y.; Luo, D.; Kou, X.-X.; Wang, X.-D.; Tay, F. R.; Sha, Y.-L.; Gan, Y.-H.; Zhou, Y.-H. Hierarchical Intrafibrillar Nanocarbonated Apatite Assembly Improves the Nanomechanics and Cytocompatibility of Mineralized Collagen. *Adv. Funct. Mater.* **2013**, *23*, 1404–1411.
44. Vestergaard, A.; Ivarsen, A. R.; Asp, S.; Hjortdal, J. Ø. Small-Incision Lenticule Extraction for Moderate to High Myopia: Predictability, Safety, and Patient Satisfaction. *J. Cataract Refractive Surg.* **2012**, *38*, 2003–2010.
45. Zimmermann, D. R.; Trüeb, B.; Winterhalter, K. H.; Witmer, R.; Fischer, R. W. Type Vi Collagen Is a Major Component of the Human Cornea. *FEBS Lett.* **1986**, *197*, 55–58.
46. Fang, M.; Goldstein, E. L.; Turner, A. S.; Les, C. M.; Orr, B. G.; Fisher, G. J.; Welch, K. B.; Rothman, E. D.; Banaszak Holl, M. M. Type I Collagen D-Spacing in Fibril Bundles of Dermis, Tendon, and Bone: Bridging between Nano-and Micro-Level Tissue Hierarchy. *ACS Nano* **2012**, *6*, 9503–9514.
47. Fang, M.; Holl, M. M. B. Variation in Type I Collagen Fibril Nanomorphology: The Significance and Origin. *BoneKEy Rep.* **2013**, 2.
48. Kadler, K.; Holmes, D.; Trotter, J.; Chapman, J. Collagen Fibril Formation. *Biochem. J.* **1996**, *316*, 1–11.
49. Dong, M.; Xu, S.; Bünger, M. H.; Birkedal, H.; Besenbacher, F. Temporal Assembly of Collagen Type Ii Studied by Atomic Force Microscopy. *Adv. Eng. Mater.* **2007**, *9*, 1129–1133.
50. Jiang, F.; Hörber, H.; Howard, J.; Müller, D. J. Assembly of Collagen into Microribbons: Effects of Ph and Electrolytes. *J. Struct. Biol.* **2004**, *148*, 268–278.
51. Bettelheim, F. A.; Plessy, B. The Hydration of Proteoglycans of Bovine Cornea. *Biochim. Biophys. Acta, Gen. Subj.* **1975**, *381*, 203–214.
52. Hatami-Marbini, H.; Etebu, E.; Rahimi, A. Swelling Pressure and Hydration Behavior of Porcine Corneal Stroma. *Curr. Eye Res.* **2013**, *38*, 1124–1132.
53. Rand, R. P. Mechanical Properties of the Red Cell Membrane: II. Viscoelastic Breakdown of the Membrane. *Biophys. J.* **1964**, *4*, 303–316.
54. Dulińska, I.; Targosz, M.; Strojny, W.; Lekka, M.; Czuba, P.; Balwierz, W.; Szymoński, M. Stiffness of Normal and Pathological Erythrocytes Studied by Means of Atomic Force Microscopy. *J. Biochem. Biophys. Methods* **2006**, *66*, 1–11.
55. Alcaraz, J.; Buscemi, L.; Grabulosa, M.; Trepat, X.; Fabry, B.; Farré, R.; Navajas, D. Microrheology of Human Lung Epithelial Cells Measured by Atomic Force Microscopy. *Biophys. J.* **2003**, *84*, 2071–2079.
56. Smith, B. A.; Tolloczko, B.; Martin, J. G.; Grütter, P. Probing the Viscoelastic Behavior of Cultured Airway Smooth Muscle Cells with Atomic Force Microscopy: Stiffening Induced by Contractile Agonist. *Biophys. J.* **2005**, *88*, 2994–3007.
57. Schoeller, D. A. Changes in Total Body Water with Age. *Am. J. Clin. Nutr.* **1989**, *50*, 1176–1181.
58. Polse, K. A.; Brand, R.; Mandell, R.; Vastine, D.; Demartini, D.; Flom, R. Age Differences in Corneal Hydration Control. *Invest. Ophthalmol. Visual Sci.* **1989**, *30*, 392–399.
59. Fisher, R. F. The Influence of Age on Some Ocular Basement Membranes. *Eye* **1987**, *1*, 184–189.
60. Hollman, K. W.; O'Donnell, M.; Erpelding, T. N. Mapping Elasticity in Human Lenses Using Bubble-Based Acoustic Radiation Force. *Exp. Eye Res.* **2007**, *85*, 890–893.
61. Elsheikh, A.; Wang, D.; Brown, M.; Rama, P.; Campanelli, M.; Pye, D. Assessment of Corneal Biomechanical Properties and Their Variation with Age. *Curr. Eye Res.* **2007**, *32*, 11–19.
62. Malik, N. S.; Moss, S. J.; Ahmed, N.; Furth, A. J.; Wall, R. S.; Meek, K. M. Ageing of the Human Corneal Stroma: Structural and Biochemical Changes. *Biochim. Biophys. Acta, Mol. Basis Dis.* **1992**, *1138*, 222–228.